Supporting Information:

Electric-Field Enhancements in Water-Dissociation Catalysis on Oxide Surfaces

T. Nathan Stovall[1,2], Justin C. Bui[2,3,4] Yifan Wu[2,4], Shujin Hou[2,4], Shannon W. Boettcher[1,2,4*], and Adam Z. Weber[2*]

[1]Department of Chemistry
University of California, Berkeley
Berkeley, CA 94720, USA

[2]Energy Technologies Area
Lawrence Berkeley National Laboratory
Berkeley, CA 94720, USA

[3]Department of Chemical and Biomolecular Engineering
NYU Tandon School of Engineering
Brooklyn, NY 11201, USA

[4]Department of Chemical and Biomolecular Engineering
University of California, Berkeley
Berkeley, CA 94720, USA

Supplementary Note 1: Basic thermodynamics of ionic processes in bipolar membranes.

Bipolar membranes (BPMs) form an ionic heterojunction upon the lamination of a cation and anion-exchange ionomeric materials. Understanding the simplest thermodynamics of this interface is valuable for the discussion of water dissociation (WD) kinetics within the BPM. Here, we will build up these basic thermodynamics as a pedagogical aid towards understanding the arguments put forth in the main manuscript.

Upon formation of the BPM, H^+ and OH^- spontaneously recombine in the ionic heterojunction to form H_2O. As recombination occurs excess capacitive charge in the anion and cation exchange layers (AEL and CEL, respectively) develop an electric potential (ϕ) gradient across the heterojunction. Net recombination ceases upon reaching the point at which the free-energy gradient imparted via a concentration gradient counterbalances the free-energy gradient imparted via an electric potential gradient, thereby nulling the total electrochemical potential ($\bar{\mu}_i^{\alpha}$) difference of each species i in phase α (*i.e.*, the spatial derivative of the electrochemical potential is zero; the definition of electrochemical equilibrium) across the heterojunction. For example, if we take H^+ as a case study, the electrochemical potential ($\bar{\mu}_i^{\alpha}$, where i is the species and α is the phase) is the same in both the CEL and AEL (**Equation S1**). Expanding out the electrochemical potentials (**Equations S2-S3**) we can solve for the difference in ϕ between the two phases given some concentration difference between the bulk membrane phases (**Equation S4**). Similarly, we can recast **Equation S4** to be in terms of the pH difference across the heterojunction, which gives an approximately 0.8 V electric potential difference between the CEL and AEL at 298 K (**Equation S5**). Notably, this does not directly give the profile through the heterojunction, and only the values at the boundary conditions.

$$\bar{\mu}_{\mathrm{H}^+,eq}^{\mathrm{CEL}} = \bar{\mu}_{\mathrm{H}^+,eq}^{\mathrm{AEL},} \tag{S1}$$

$$\bar{\mu}_i^{\alpha} = \mu^0 + \frac{RT}{nF}\ln(a_i) + zF\phi^{\alpha} \tag{S2}$$

$$\mu_{\mathrm{H}^+}^0 + \frac{RT}{F}\ln(a_{\mathrm{H}^+,eq}^{\mathrm{CEL}}) + F\phi^{\mathrm{CEL}} = \mu_{\mathrm{H}^+}^0 + \frac{RT}{F}\ln(a_{\mathrm{H}^+,eq}^{\mathrm{AEL}}) + F\phi^{\mathrm{AEL}} \tag{S3}$$

$$\Delta\phi_{eq} = \phi_{eq}^{\mathrm{CEL}} - \phi_{eq}^{\mathrm{AEL}} = \frac{RT}{F}\ln\left(\frac{a_{\mathrm{H}^+,eq}^{\mathrm{AEL}}}{a_{\mathrm{H}^+,e}^{\mathrm{CEL}}}\right) \tag{S4}$$

$$\phi_{eq}^{\mathrm{CEL}} - \phi_{eq}^{\mathrm{AEL}} = \frac{-\ln(10)\,RT}{F}\left(\mathrm{pH}_{eq}^{\mathrm{AEL}} - \mathrm{pH}_{eq}^{\mathrm{CEL}}\right) \approx -0.8\,V\ (@\ T = 298\ \mathrm{K}) \tag{S5}$$

From these results it is evident that there will be a large potential drop through the WD catalyst layer thereby imparting a large electric field. However, the work done above *does not* account for any ionic and electronic character in the WD catalyst layer. In the main manuscript, we discuss extensively how the electric potential within the catalyst layer is highly non-trivial and is a function of the electronic and ionic properties of the catalyst layer.

When a bias is applied the BPM is driven out of equilibrium and there exists a thermodynamic driving force for WD or H^+/OH^- recombination if the transmembrane bias is increased or decreased, respectively. For example, if the transmembrane electric potential is increased across the heterojunction (reverse-bias) $\bar{\mu}_{H^+}^{CEL}$ is reduced relative to $\bar{\mu}_{H^+}^{AEL}$ (**Equation S6**) ultimately providing a driving force for the expulsion of H^+ out of the heterojunction. In this case, the electrochemical potential gradient due to an electric potential gradient exceeds that of the concentration (or activity) gradients (**Equation S7**). We remind the reader that the flux of species i ($\boldsymbol{N}_i$) arises from gradients in $\bar{\mu}_i^{\alpha}$ (**Equation S8**). The activities given here can be considered of the bulk membrane phases. Within the bipolar junction, the chemical potential of species is not necessarily constant as a function of applied bias, as the relative H^+ and OH^- concentrations likely change.

$$\mu_{H^+}^0 + \frac{RT}{F}\ln(a_{H^+,eq}^{CEL}) + F\phi^{CEL} < \mu_{H^+}^0 + \frac{RT}{F}\ln(a_{H^+,eq}^{AEL}) + F\phi^{AEL} \quad (\mathbf{S6})$$

$$F\left(\phi^{CEL} - \phi^{AEL}\right) > RT\ln\left(\frac{a_{H^+}^{AEL}}{a_{H^+}^{CEL}}\right) \quad (\mathbf{S7})$$

$$\boldsymbol{N_i} = -\frac{c_i D_i}{RT}\left(\frac{\partial \bar{\mu}_i}{\partial x}\right) \quad (\mathbf{S8})$$

In the case of forward-bias, the concentration gradients exceed the electric potential gradients, thereby imparting an inward flux of H^+ and OH^- to the heterojunction (**Equation S9-S10**).

$$\mu_{H^+}^0 + \frac{RT}{F}\ln(a_{H^+,eq}^{CEL}) + F\phi^{CEL} > \mu_{H^+}^0 + \frac{RT}{F}\ln(a_{H^+,eq}^{AEL}) + F\phi^{AEL} \quad (\mathbf{S9})$$

$$F\left(\phi^{CEL} - \phi^{AEL}\right) < RT\ln\left(\frac{a_{H^+}^{AEL}}{a_{H^+}^{CEL}}\right) \quad (\mathbf{S10})$$

The physics detailed here provides the most basic underlying physics to understand the physics of the bipolar junction. We point the reader to a simple continuum model that has been developed by Chen *et al.*,[1] to demonstrate the physics of the BPM. For more advanced modeling efforts, we point the reader to the works of Bui *et al.*[2,3]

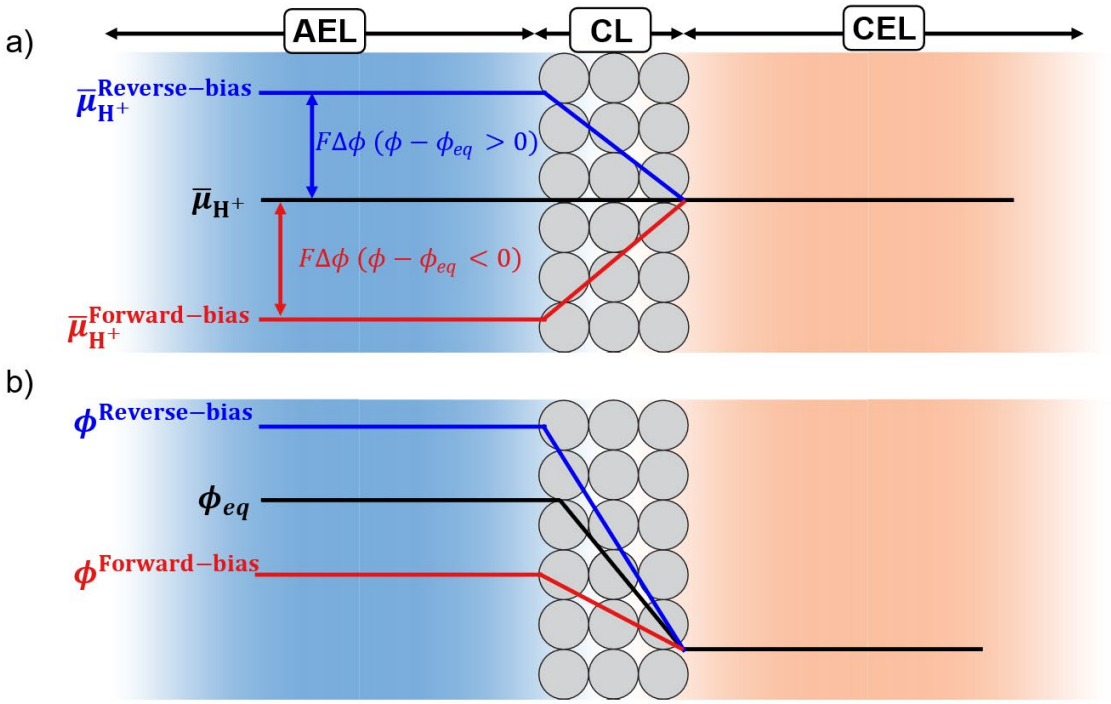

Figure S1: Basic physics of BPMs in forward and reverse bias. (a) The gradient in electrochemical potential of each species is zero at equilibrium. Under an electric bias, the electrochemical potential of charged species respond, creating a thermodynamic driving force for charge transport. **(b)** Increasing the electric potential across the BPM affords a driving force for reverse-bias current, and decreasing the transmembrane electric potentials drives forward-bias current, given sufficient kinetic facility.

Supplementary Note 2: Membrane potential sensing in membrane electrode assemblies.

In this work we deployed a membrane potential sensing testbed to measure the transmembrane potential (and subsequently WD overpotential) across the BPM. Here, we will discuss precisely what membrane potential sensing measures.

Here, we use a Hg|HgO reference electrode on the AEL side and saturated calomel electrode (SCE) at the CEL. First, we will consider only the SCE reference electrode. SCE reference electrodes have their potential pinned via the redox reaction shown in Reaction S1.

$$\mathrm{Hg_2Cl_2}\ (s) + 2\ \mathrm{e^-} \rightleftharpoons 2\ \mathrm{Hg}\ (\ell) + 2\ \mathrm{Cl^-}(aq) \qquad E^0_{SCE} = 0.241\ \mathrm{V\ vs\ SHE} \tag{S11}$$

A potentiostat (or voltmeter) always measures the electrochemical potential of an electron in some metal phase (*not electric potentials*). Thus, for the SCE reference electrode, it is the electrochemical potential of the electron being reported by the reference electrode. Assuming the reference electrode is at equilibrium we can write the electrochemical potential of the electron as shown in **Equation S11**.

$$\bar{\mu}_{e^-}^{\mathrm{SCE}} = \bar{\mu}_{\mathrm{Cl^-}}^{\mathrm{SCE}} + \mu_{\mathrm{Hg}}^{\mathrm{SCE}} - \frac{1}{2}\mu_{\mathrm{Hg_2Cl_2}}^{\mathrm{SCE}} \tag{S12}$$

Expanding out the electrochemical potential for Cl, and combining all terms that are agnostic to electric potential into μ_{all}, we find that the electrochemical potential of the electron is a function of the electric potential felt by Cl^- (**Equation S12**). The solution electric potential felt by the Cl^- is equivalent to the electric potential in the CEL, as the concentrated reference solution creates a negligible junction potential between the reference solution and the membrane. The activity of species are nominally constant in the reference electrode, thus the chemical potentials are all also constant.

$$\bar{\mu}_{e^-}^{\mathrm{SCE}} = \mu_{all}^{\mathrm{SCE}} - F\phi^{\mathrm{CEL}} \tag{S13}$$

We can similarly write the following relationship using identical steps with the Hg|HgO reference electrode on the AEL side **(Equation S13**).

$$\bar{\mu}_{e^-}^{\mathrm{Hg|HgO}} = \mu_{all}^{\mathrm{Hg|HgO}} - F\phi^{\mathrm{AEL}} \tag{S14}$$

We report the measured potential as the difference between the AEL and CEL reference electrodes (arbitrarily chosen to provide positive potential values). Thus, we can take the difference between the electrochemical potentials of the electrons in each electrode and find the difference is proportional to some constant difference in chemical potential and the difference in electric potential between each membrane phase (**Equation S14**).

$$-\left(\frac{\bar{\mu}_{e^-}^{\mathrm{Hg|HgO}} - \bar{\mu}_{e^-}^{\mathrm{SCE}}}{F}\right) = -\frac{\Delta\mu_{all}}{F} + \phi^{\mathrm{AEL}} - \phi^{\mathrm{CEL}} \tag{S15}$$

From this we find that the reference electrodes affixed to the membrane can report on the electric potential difference across the membrane *indirectly*. That is, we are not rigorously measuring

electric potential but instead can use the electrochemical potential of the electrons as a proxy for the electric potential felt by the ions. The constant chemical-potential offset is the correction for the different standard potentials of the two reference electrodes. When we take our measured potential at a given current and subtract the open-circuit potential to recover the overpotential, the difference in chemical potentials cancel. Notably, the measured membrane potentials are sensitive to various undesirable excess chemical potentials (for example, due to membrane hydration, hydroxide/CO_2 equilibria in exposed AEM strip, etc…) that results in measurement error. Again, assuming these excesses are time-independent (which is normally true for short experiments) they should cancel following subtraction of the open-circuit potential. It is also important to ensure some hydration in the membranes to ensure ionic conductivity is maintained. When reporting absolute measured potentials, or performing long experiments where the reference potential is likely to drift, it is best practice to calibrate the reference electrode *in-situ* with an internal known standard, for example, versus the cathode which can be poised to the hydrogen potential and act as an RHE.

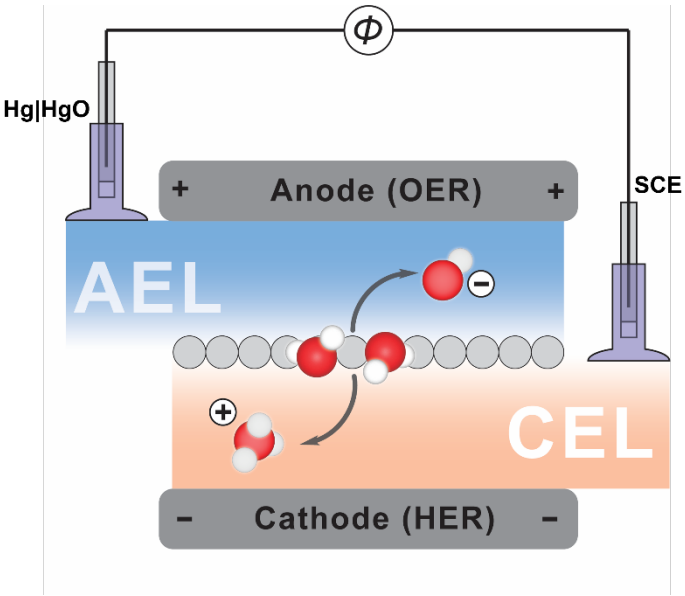

Figure S2: Membrane potential sensing testbed. The membrane potential sensing employed here using AEL and CEL reference strips affixed to Hg|HgO and SCE reference electrodes, respectively, enabling the measurement of transmembrane potential across the reference electrodes.

Supplementary Note 3: Connecting entropy and enthalpy to the Arrhenius analysis

Temperate-dependent kinetic measurements and subsequent Arrhenius analyses provide insights into the apparent entropic and enthalpic contributions to reaction transition-state barriers. The Arrhenius equation (**Equation S16**) is a phenomenological relationship that describes the temperature dependence of a chemical reaction rate (constant), where k is the rate constant, A is the Arrhenius prefactor, R is the ideal-gas constant, T is absolute temperature and E_a is the activation barrier.

$$k = A \exp\left(-\frac{E_a}{RT}\right) \tag{S16}$$

A more thermodynamically explicit formulation of chemical kinetics is the Eyring-Polanyi equation (**Equation S17**) which is grounded in transition-state-theory. In this framework, rate is expressed in terms of the free-energy difference between the reactant and transition states, where κ is the transmission coefficient, which accounts for recrossing over the transition state, k_B is the Boltzmann constant, h is Planck's constant, and $\Delta G^{\ddagger}$ is the Gibbs free energy of activation of the transition state.

$$k = \kappa \frac{k_B T}{h} \exp\left(-\frac{\Delta G^{\ddagger}}{RT}\right) \tag{S17}$$

Separating the free energy of activation into its enthalpic and entropic components yields

$$k = \kappa \frac{k_B T}{h} \exp\left(\frac{\Delta S^{\ddagger}}{R}\right) \exp\left(-\frac{\Delta H^{\ddagger}}{RT}\right) \tag{S18}$$

From this expression, we can analyze it a couple of ways. One is to write the effective Arrhenius prefactor as

$$A(T) \equiv \kappa \frac{k_B T}{h} \exp\left(\frac{\Delta S^{\ddagger}}{R}\right) \tag{S19}$$

and then by inspection we would have

$$E_a = \Delta H^{\ddagger} \tag{S20}$$

In this approach, unlike the Arrhenius equation, the Eyring equation explicitly suggests a weak linear temperature dependence to the prefactor. However, this effect is often sufficiently small such that a quasi-temperature-independent prefactor is often reasonably invoked.

A second approach would be to lump the T-dependent and -independent terms of Equation S18 such that

$$A \equiv \kappa \frac{k_B}{h} \exp\left(\frac{\Delta S^{\ddagger}}{R}\right) \tag{S21}$$

Then differentiating as per an Arrhenius plot and analysis where E_a is taken to be the slope of $\ln(k)$ versus $1/T$,

$$E_a \equiv -R\left(\frac{d\ln(k)}{d\left(\frac{1}{T}\right)}\right) \quad \textbf{(S22)}$$

From this we can recover E_a to be the enthalpic barrier plus thermal energy:

$$E_a = \Delta H^{\ddagger} + RT \quad \textbf{(S23)}$$

Thus, either analysis demonstrates that the prefactor relates to entropy and the activation barrier to enthalpy. This analysis is the basis for using A as proxy for the entropic barrier and E_a as a proxy for the enthalpic barrier in the main text. We remind the reader that these entropic and enthalpic barriers are the difference between the transition state and ground state (**Equations S24** and **25**):

$$\Delta S^{\ddagger} = S^{\ddagger} - S^{reactant} \quad \textbf{(S24)}$$

$$\Delta H^{\ddagger} = H^{\ddagger} - H^{reactant} \quad \textbf{(S25)}$$

In the case of TiO_2, we hypothesize that increasing interfacial electric fields induces ordering of interfacial water thereby reducing the configurational entropy of the reactant ensemble. If this order disproportionately constrains the reactant ensemble relative to the (already highly constrained) transition state, the apparent Arrhenius prefactor should increase (*e.g.*, the entropic barrier was reduced, and $\Delta S^{\ddagger}$ becomes more positive).

Likewise, at sufficiently large electric fields (and already pre-organized water) as in the case of GO_x, we hypothesize potential enthalpic effects. Electric fields can increase the effective acidity of interfacial water by stabilizing dipole-aligned configurations, and can also electrostatically stabilize the highly polar transition state associated with ion-transfer reactions. However, as discussed in the main text, the exceedingly large field-dependence of the GO_x water dissociation catalyst seemingly cannot be explained via simple electrostatic stabilization of the O-H bond. Thus, further investigations are needed.

Supplementary Figures S3-S9

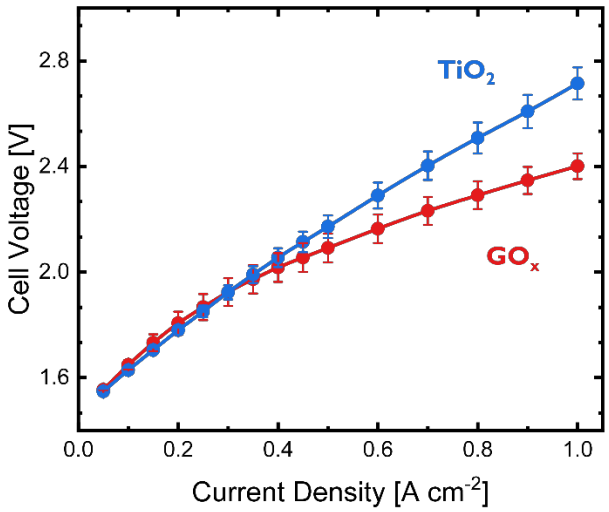

Figure S3: Full cell polarization curve of BPM water electrolyzer. The full cell polarization signature for both GO_x and TiO_2 water dissociation catalysts, again demonstrating the increased curvature of the GO_x *i-V* response. The electrolyzer cell included an IrO_2 anode and Pt/C (45 wt% Pt) cathode and was operated at 55°C.

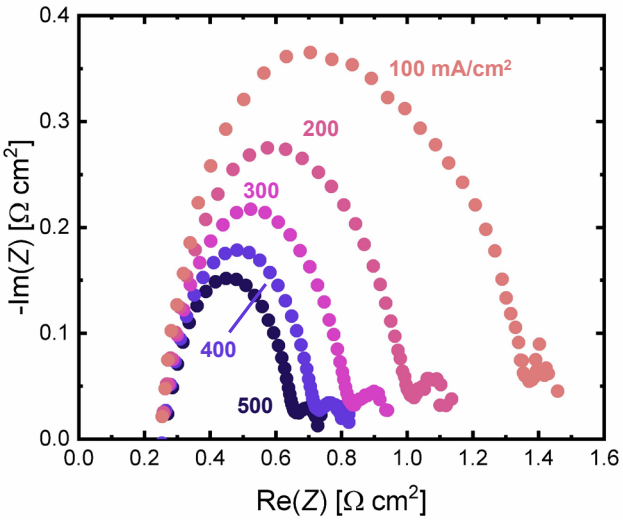

Figure S4: Current-dependent full-cell impedance spectra of GO_x BPM.
Impedanc

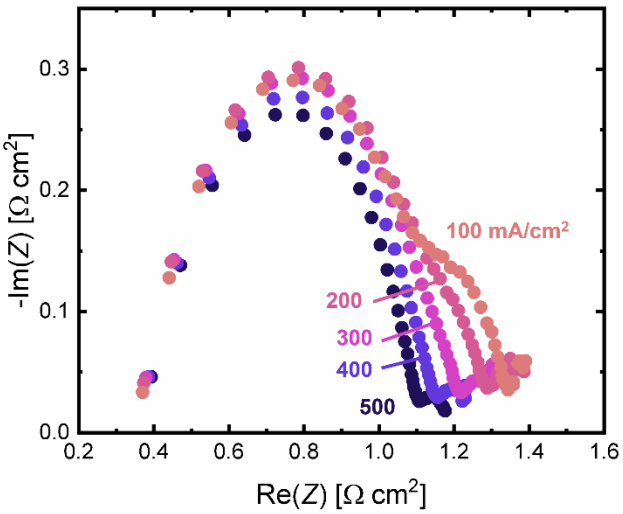

Figure S5: Current-dependent full-cell impedance spectra of TiO_2 BPM.
Impedance spectra of TiO_2 BPM water electrolyzer operated at 55°C.

The high frequency semi-circle in the Nyquist plot we believe to be a combination of an electrode charge-transfer process as well as WD (in the low current regime, the semicircle begins to split into two). We chose not to fit the semicircles due to the high degree of overlap making the fits highly subjective. Nonetheless, we find that the GO_x impedance response is significantly more sensitive to the applied current density (or operative potential), manifesting in a significant

reduction in high frequency charge-transfer resistance. For TiO_2 we see a much smaller reduction, as the WD impedance is likely insensitive to bias.

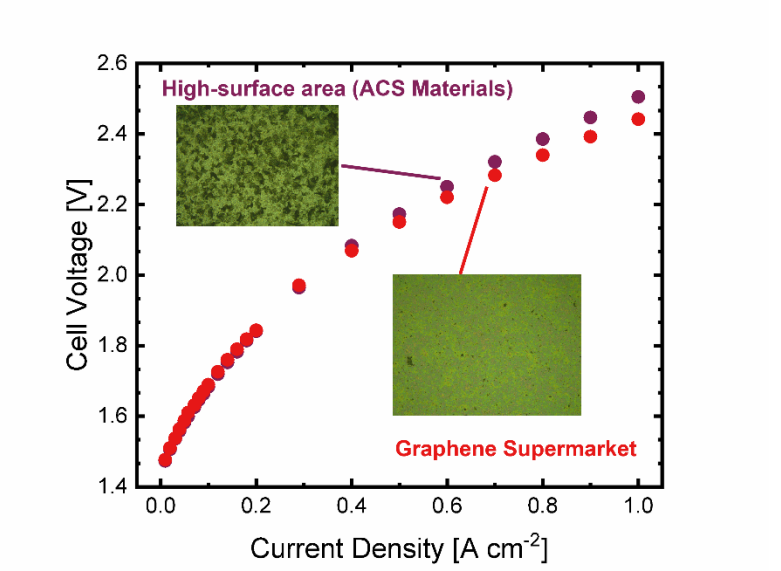

Figure S6: Polarization curves with differing catalyst layer morphology. Nearly-identical performance was observed for two GO_x catalyst layers with drastically different morphology and flake size. Data collected using 5 cm^2 active area at 55 °C.

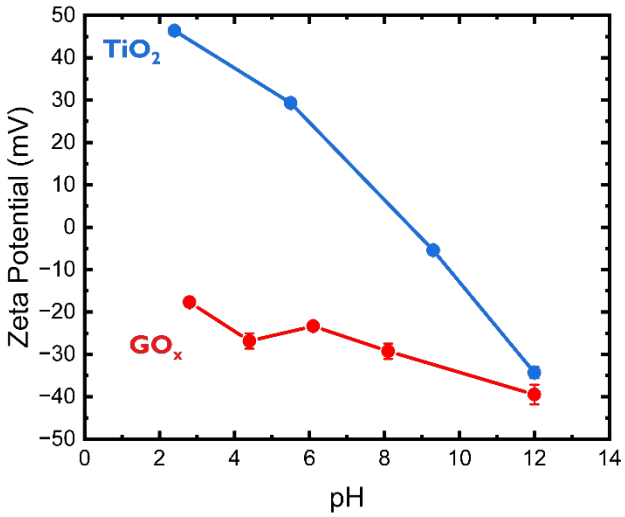

Figure S7: pH-dependent zeta-potential measurements. The zeta-potential of GO_x and TiO_2 WD catalysts demonstrate the high acidity of GO_x at all pH values relative to TiO_2 which has a surface with wide range of acid/base sites which (de)protonate at varying pHs.

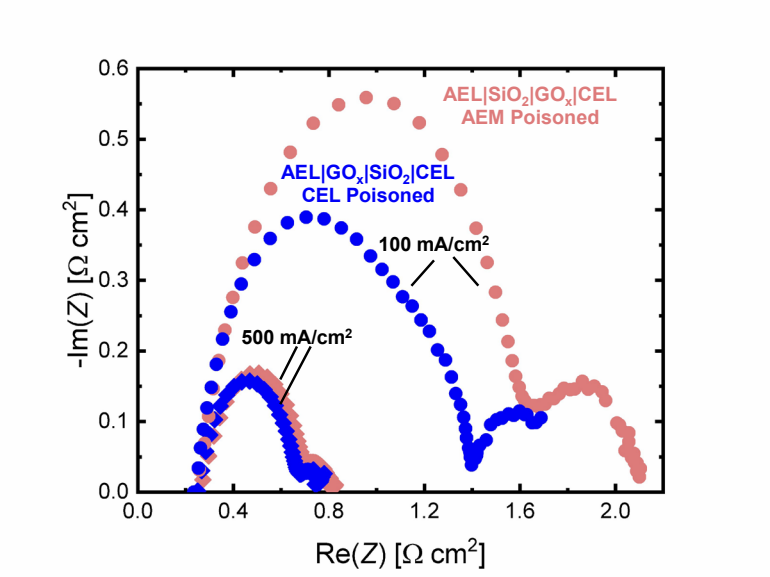

Figure S8: Impedance response of GO_x BPMs poisoned with SiO_2 on CEL and AEL. The impedance spectra show reduced total charge transfer resistance when the BPM is poisoned on the CEL side relative to the AEL side. The difference in charge transfer resistance decreases at higher current densities, possibly due to a sufficient electric field being developed with the excess applied potential.

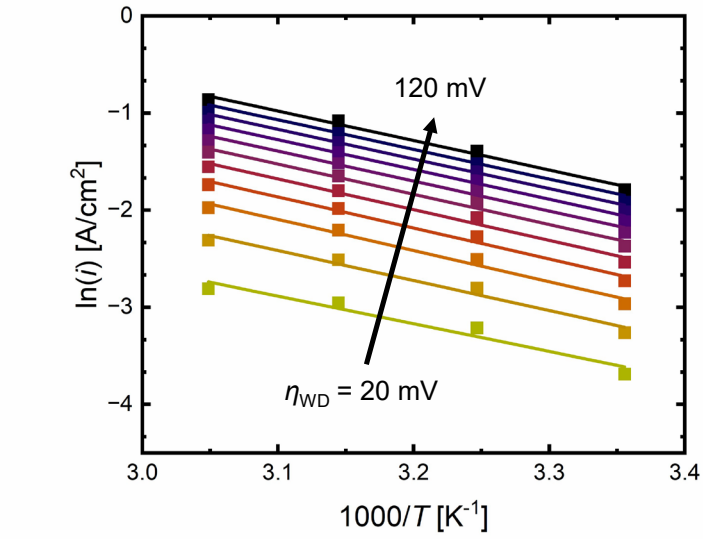

Figure S9: Example Arrhenius plot for TiO_2 BPM.

References

(1) Chen, L.; Xu, Q.; Oener, S. Z.; Fabrizio, K.; Boettcher, S. W. Design principles for water dissociation catalysts in high-performance bipolar membranes. *Nat. Commun.* **2022**, *13* (1), 3846. DOI: 10.1038/s41467-022-31429-7.
(2) Bui, J. C.; Lucas, É.; Lees, E. W.; Liu, A. K.; Atwater, H. A.; Xiang, C.; Bell, A. T.; Weber, A. Z. Analysis of bipolar membranes for electrochemical CO2capture from air and oceanwater. *Energy Environ. Sci.* **2023**, *16* (11), 5076-5095. DOI: 10.1039/d3ee01606d.
(3) Bui, J. C.; Corpus, K. R. M.; Bell, A. T.; Weber, A. Z. On the Nature of Field-Enhanced Water Dissociation in Bipolar Membranes. *J. Phys. Chem. C* **2021**, *125* (45), 24974-24987. DOI: 10.1021/acs.jpcc.1c08276.